Environmental Science & Technology

Article

Cite This: Environ. Sci. Technol. 2018, 52, 11769−11777

pubs.acs.org/est

Hydrothermal Stability of CeO_2−WO_3−ZrO_2 Mixed Oxides for Selective Catalytic Reduction of NOx by NH_3

Jingjing Liu,[†,§] Xiaoyan Shi,[†,§] Yulong Shan,[†,§] Zidi Yan,[†,§] Wenpo Shan,[‡] Yunbo Yu,[†,‡,§] and Hong He*[,†,‡,§]

[†]State Key Joint Laboratory of Environment Simulation and Pollution Control, Research Center for Eco-Environmental Sciences, Chinese Academy of Sciences, Beijing 100085, China

[‡]Center for Excellence in Regional Atmospheric Environment, Institute of Urban Environment, Chinese Academy of Sciences, Xiamen 361021, China

[§]University of Chinese Academy of Sciences, Beijing 100049, China

Supporting Information

ABSTRACT: CeO_2−WO_3−ZrO_2 mixed oxides were prepared by the homogeneous precipitation method for the selective catalytic reduction of NOx with NH_3 (NH_3−SCR). The effects of hydrothermal aging on the catalytic performances of CeO_2−WO_3−ZrO_2 were investigated. The results showed that CeO_2−WO_3−ZrO_2 catalyst exhibited excellent NH_3−SCR activity for removal of NOx and hydrothermal stability. After hydrothermal aging at 850 °C for 16 h, the optimum CeO_2−WO_3−ZrO_2 catalyst could still realize 80% NOx conversion at 300−500 °C even under a high gas hourly space velocity of 250 000 h^{-1}. The structural properties, redox ability, surface species, and acidity of fresh and hydrothermally aged CeO_2−WO_3−ZrO_2 catalysts were characterized by N_2-physisorption, XRD, Raman, H_2-TPR, XPS, NH_3-TPD, and *in situ* DRIFTS. The characterization results showed that decreases of 89% of the surface area and 71% of the NH_3 storage capacity as well as new phase formation occurred for the CeO_2−WO_3−ZrO_2 sample after hydrothermal aging at 850 °C for 16 h. The activity of hydrothermally aged CeO_2−WO_3−ZrO_2 was mainly attributed to the retention of redox-acid sites and their interaction due to the formation of Ce−Zr solid solutions and $Ce_4W_9O_{33}$.

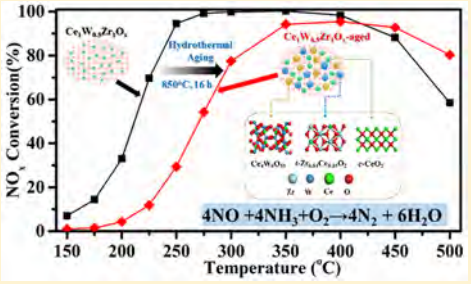

1. INTRODUCTION

The selective catalytic reduction of NOx with NH_3 (NH_3−SCR) is an efficient technology for NOx removal from diesel engines. Besides high de-NOx efficiency, excellent hydrothermal stability up to 800 °C is also critical for SCR catalysts in diesel emission control, since water always emits from internal combustion engines and the regeneration of DPF exposes the SCR catalysts to a high temperature.[1,2] Recently, mixed oxides, such as Ce- and Fe-based catalysts, have been widely studied for NH_3−SCR of NOx.[3] However, the hydrothermal stability of mixed oxides is questionable for practical application in diesel after-treatment systems.[4] Ceria−zirconium mixed oxides are well-known for their outstanding thermal stability.[5] The SCR activity of ceria−zirconium mixed oxides can be improved by the addition of acidic components, for example, $Ce_{0.75}Zr_{0.25}O_2$−PO_4^{3-},[6] WO_3/ZrO_2−$Ce_{0.6}Zr_{0.4}O_2$,[7] CeO_2−WO_3−ZrO_2,[8−10] and NbO_x−CeO_2−ZrO_2.[11] These acidity-promoted ceria−zirconium mixed oxides showed outstanding activity for the NH_3−SCR reaction, and some of these catalysts have been reported to exhibit excellent hydrothermal stability.[10,11] For instance, 80% of NOx conversion was still obtained above 300 °C over a $Ce_1Nb_{3.0}Zr_2O_x$ catalyst after it was hydrothermally treated at 800 °C for 48 h under a GHSV of 50 000 h^{-1}.[11] Therefore, the acidity-promoted ceria−zirconium oxides are promising candidates for the abatement of NOx from diesel vehicles.[1,11]

WO_3-doped Ce−Zr solid solutions as well as CeO_2−WO_3−ZrO_2 mixed oxides have been studied for NH_3−SCR of NOx.[7−10,12] A 10 wt % WO_3/CeO_2−ZrO_2 catalyst, which was prepared by impregnating WO_3 on CeO_2−ZrO_2, showed nearly 100% NOx conversion within the range 200−500 °C.[12] Ning et al. reported that higher NOx conversion can be obtained over CeO_2−WO_3−ZrO_2 catalysts prepared by hydrothermal or coprecipitation methods, while samples prepared by impregnating WO_3 on CeO_2−ZrO_2 exhibited relatively poor SCR activity.[9] Song et al. reported that hydrothermally synthesized CeO_2−WO_3−ZrO_2 catalysts were stable after being hydrothermally aged at 700−900 °C for 8 h and attributed the hydrothermal stability of the catalyst at 700 °C to its remaining redox properties and highly dispersed or amorphous WO_3 species after hydrothermal-aging treatment.[10] However, the results in their report cannot satisfactorily explain why CeO_2−WO_3−ZrO_2 catalysts hydrothermally aged at 800 °C for 8 h still

Received: July 6, 2018
Revised: September 4, 2018
Accepted: September 12, 2018
Published: September 12, 2018

DOI: 10.1021/acs.est.8b03732
Environ. Sci. Technol. 2018, 52, 11769−11777

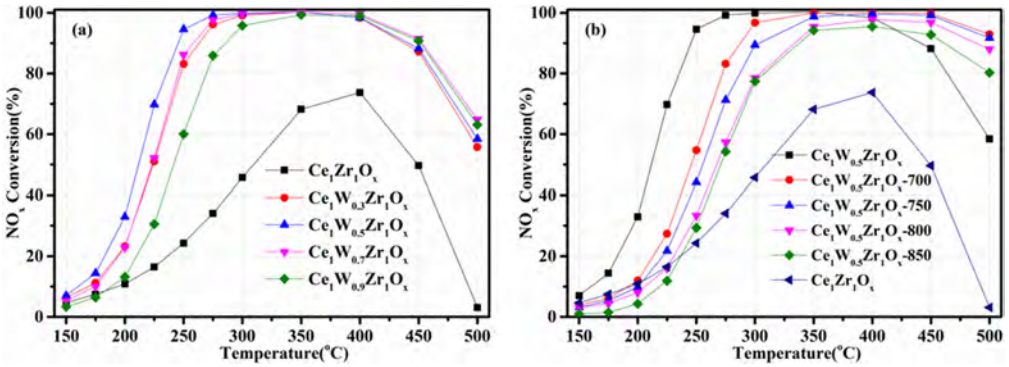

Figure 1. Effects of W/Ce molar ratio (a) and hydrothermal aging temperature (b) on the NOx conversion over catalysts. Reaction conditions: [NO] = [NH_3] = 500 ppm, [O_2] = 5 vol %, balance N_2, and GHSV = 250 000 h^{-1}.

realized ~100% NOx conversion at 300−500 °C, even after the formation of a new tungsten-containing crystal phase.[10] Recently, Iwasaki et al. pointed out that the much higher SCR reactivity of WO_3/CeO_2 than that of a mixture of WO_3/ZrO_2 and CeO_2 could be mainly attributed to the atomic-scale site proximity and large amount of acidic-redox site interfaces.[13] In order to understand the hydrothermal stability of CeO_2−WO_3−ZrO_2, a systematic study on the phase transformation that occurs during the interaction of WO_3, CeO_2, and ZrO_2, including formation of the Ce−Zr oxide solid solutions and cerium tungstates, and the number of active sites remaining for the SCR reaction (redox-acidic sites) after hydrothermal aging at high temperature, needs to be carried out.

In this work, a series of CeO_2−WO_3−ZrO_2 catalysts with different W/Ce molar ratios were prepared by a homogeneous precipitation method. The CeO_2−WO_3−ZrO_2 catalyst was hydrothermally aged at 700, 750, 800, and 850 °C for 16 h. The effects of hydrothermal aging on the SCR activity and the interaction between WO_3, CeO_2, and ZrO_2 in CeO_2−WO_3−ZrO_2 catalysts were investigated.

2. MATERIALS AND METHODS

2.1. Catalyst Preparation and Hydrothermal Aging Treatment. The CeO_2−WO_3−ZrO_2 catalysts with the required molar ratios (Ce/W/Zr = 1:*a*:1, where *a* = 0.3, 0.5, 0.7, and 0.9) were synthesized by a homogeneous precipitation method using urea as the precipitant. Synthesis details can be found in the Supporting Information. The obtained catalysts were denoted as $Ce_1W_aZr_1O_x$. For comparison, CeO_2, ZrO_2, and $Ce_1Zr_1O_x$ samples were also prepared by the same method. The obtained catalysts were pressed, crushed, and sieved to 40−60 mesh for SCR activity testing.

The selected samples, $Ce_1W_{0.5}Zr_1O_x$ and $Ce_1Zr_1O_x$, were hydrothermally aged in 10 vol % H_2O/air at 700, 750, 800, and 850 °C, respectively, for 16 h and denoted as $Ce_1W_{0.5}Zr_1O_x$-T and $Ce_1Zr_1O_x$-T, where "T" represents the hydrothermal aging temperature.

2.2. Catalytic Activity Test. The NH_3−SCR activity measurements were carried out in a fixed-bed quartz tube flow reactor with inner diameter of 4 mm. The flue gas composition was as follows: 500 ppm of NO, 500 ppm of NH_3, 5% O_2, and balance N_2. Reactant gases were regulated by mass-flow controllers before entering the reactor. The concentrations of NH_3, NO, NO_2, and N_2O were continually monitored by an FTIR spectrometer (IS10 Nicolet), which was equipped with a multiple path gas cell (2 m).

The NOx conversion and N_2 selectivity were calculated as follows:

$$\text{NOx conversion} = \left(1 - \frac{[NO_x]_{out}}{[NO_x]_{in}}\right) \times 100\% \quad (1)$$

$$N_2 \text{ selectivity} = \left(1 - \frac{2[N_2O]_{out}}{([NO_x]_{in} - [NO_x]_{out}) + ([NH_3]_{in} - [NH_3]_{out})}\right) \times 100\% \quad (2)$$

where [NOx] = [NO] + [NO_2], $[NOx]_{in}$, and $[NOx]_{out}$ denote the inlet and outlet gas concentrations of NOx, respectively.

2.3. Kinetic Studies. The kinetic experiments for standard SCR were evaluated in the same fixed-bed reactor as the activity test. The NOx conversion was kept at less than 20% in the temperature range of 200−260 °C. The reaction rates of NO conversion ($-R_{NOx}$, in mol m^{-2} s^{-1}), normalized by the surface area, were calculated as follows:[13,14]

$$-R_{NO_x} = \frac{F_{NO_x} \times x}{W \times S} \quad (3)$$

where F_{NO_x} is the molar flow rate of NOx (in mol s^{-1}), *x* is the conversion of NO, *W* is the weight of catalyst (in g), and *S* is the BET surface area (in m^2 g^{-1}). The apparent activation energies (E_a, in kJ mol^{-1}) can be calculated from the Arrhenius plots of the reaction rates.

2.4. Catalyst Characterization. The N_2 adsorption−desorption analysis of catalysts was carried out using a Quantachrome Autosorb-1C instrument at a liquid nitrogen temperature (−196 °C). Powder X-ray diffraction (XRD) patterns of the samples were measured on a Bruker D8 diffractometer with Cu Kα (λ = 0.15406 nm) radiation. Raman spectra of the SCR catalysts were recorded on a homemade UV resonance Raman spectrometer (UVR DLPC-DL-03) with a 532 nm laser beam He−Cd laser. The temperature-programmed reduction of hydrogen (H_2-TPR) was carried out on a Micromeritics AutoChem 2920 chemisorption analyzer. XPS measurements were carried out on an X-ray photoelectron spectrometer (AXIS Supra/Ultra) with Al Kα radiation (1486.7 eV). Temperature-programmed desorption of ammonia (NH_3-TPD) was carried out in a fixed-bed quartz tube flow reactor with an inner diameter of 4 mm, and the concentration of NH_3 was continually monitored by an FTIR spectrometer (IS10 Nicolet). The *in situ* DRIFTS experiments were performed on

DOI: 10.1021/acs.est.8b03732
Environ. Sci. Technol. 2018, 52, 11769−11777

an FTIR spectrometer (Nicolet IS50) equipped with an MCT/A detector. The experimental details can be found in the Supporting Information.

3. RESULTS AND DISCUSSION

3.1. NH_3−SCR Catalytic Activity and Textural Properties. Figure 1a depicts the NOx conversion of fresh $Ce_1Zr_1O_x$ and $Ce_1W_aZr_1O_x$ catalysts at a GHSV of 250 000 h^{-1}. The results show that $Ce_1Zr_1O_x$ exhibited low NOx conversion, with a maximum NOx conversion of 74% at 400 °C. Significant enhancement of NOx conversion was realized over $Ce_1W_aZr_1O_x$ with the addition of W into $Ce_1Zr_1O_x$. The low-temperature activity of $Ce_1W_aZr_1O_x$ (below 300 °C) was improved by increasing the W/Ce molar ratio from 0.3 to 0.5. However, when further increasing the W/Ce molar ratio to 0.7 and 0.9, the NOx conversion at low temperatures decreased. The W/Ce molar ratio in $Ce_1W_aZr_1O_x$ showed little effect on the high temperature activity (above 300 °C). For $Ce_1W_aZr_1O_x$, the N_2 selectivity was near 100% (Figure S1a). Additionally, $Ce_1W_{0.5}Zr_1O_x$ exhibited excellent NH_3−SCR activity even under a high GHSV of 500 000 h^{-1}, where over 80% NOx conversion was obtained in the range of 250−450 °C (Figure S2).

The hydrothermal stability of an SCR catalyst at high temperature is important for practical application. Here, the effects of the hydrothermal aging temperature on the catalytic performance of $Ce_1W_{0.5}Zr_1O_x$ were examined. As the results in Figure 1b show, compared to $Ce_1W_{0.5}Zr_1O_x$, an obvious decrease in the low temperature activity and enhancement of the high temperature activity were observed for $Ce_1W_{0.5}Zr_1O_x$-700. The improved activity of SCR catalysts at high temperatures after hydrothermal aging was also observed in previous studies,[10,11] and it could be associated with the decreased NH_3 oxidation activity, which would divert NH_3 from the SCR reaction.[15] Furthermore, the low-temperature activity slightly decreased with the increase of the hydrothermal aging temperature. It is worth noting that, after being severely hydrothermally aged at 850 °C for 16 h, $Ce_1W_{0.5}Zr_1O_x$-850 still exhibited higher NH_3−SCR activity than that of fresh $Ce_1Zr_1O_x$ in the temperature range of 250−500 °C. The NOx conversion of $Ce_1W_{0.5}Zr_1O_x$-850 was more than 80% in the temperature range of 300−500 °C. In addition, all the hydrothermally aged $Ce_1W_{0.5}Zr_1O_x$ catalysts possessed high N_2 selectivity in the SCR reaction, as shown in Figure S1b. The above results suggested that $Ce_1W_{0.5}Zr_1O_x$ possessed excellent hydrothermal stability.

The BET specific surface area, pore diameter, and pore volume were investigated by N_2 physisorption. As shown in Table S1, the surface areas of $Ce_1W_aZr_1O_x$ with the molar ratio of W/Ce = 0.3, 0.5, and 0.7 were higher than that of $Ce_1Zr_1O_x$. However, excessive addition of W to $Ce_1Zr_1O_x$ resulted in a severe loss of surface area. The BET surface area of $Ce_1W_{0.9}Zr_1O_x$ (49.3 m^2/g) was much lower than that of $Ce_1W_{0.5}Zr_1O_x$ (92.0 m^2/g). This result indicated that the addition of W to $Ce_1Zr_1O_x$ can affect the structural parameters of $Ce_1Zr_1O_x$ and that optimizing the W addition amount is important to obtain samples with a high surface area.

As listed in Table 1, after hydrothermal aging at 700 °C for 16 h, the surface area and pore volume of $Ce_1W_{0.5}Zr_1O_x$ decreased from 92.0 m^2/g to 16.6 m^2/g and from 0.10 cc/g to 0.05 cc/g, respectively. In addition, a sharp increase of the average pore diameter was observed for the $Ce_1W_{0.5}Zr_1O_x$-700 sample. This indicated that sintered particles and extra secondary piled pores formed in $Ce_1W_{0.5}Zr_1O_x$ after the hydrothermal aging treatment.[16] However, the surface area and pore volume of $Ce_1W_{0.5}Zr_1O_x$ declined to a small degree when further increasing the hydrothermal-aging temperature. $Ce_1W_{0.5}Zr_1O_x$-850 exhibited a surface area of 10.2 m^2/g and pore volume of 0.03 cc/g.

Table 1. Structural Parameters of $Ce_1Zr_1O_x$, $Ce_1W_{0.5}Zr_1O_x$, and $Ce_1W_{0.5}Zr_1O_x$-T Catalysts from N_2 Physisorption Results

samples	S_{BET}[a] (m^2/g)	pore diameter[b] (nm)	pore volume[c] (cc/g)	$R_S \times 10^{10}$ at 200 °C[d] ($mol/s^{-1}/m^{-2}$)
$Ce_1Zr_1O_x$	73.2	4.3	0.08	6.7
$Ce_1W_{0.5}Zr_1O_x$	92.0	4.3	0.10	23.3
$Ce_1W_{0.5}Zr_1O_x$-700	16.6	12.4	0.05	35.6
$Ce_1W_{0.5}Zr_1O_x$-750	16.1	13.0	0.05	37.2
$Ce_1W_{0.5}Zr_1O_x$-800	12.2	13.4	0.04	36.4
$Ce_1W_{0.5}Zr_1O_x$-850	10.2	13.4	0.03	35.8

[a]BET surface area. [b]Average pore diameter. [c]Total pore volume. [d]SCR reaction rates at 200 °C normalized by catalyst surface area.

The XRD patterns of CeO_2, ZrO_2, $Ce_1Zr_1O_x$, and $Ce_1W_{0.5}Zr_1O_x$ catalysts are depicted in Figure 2a. The data showed that $Ce_1Zr_1O_x$ exhibited the structures of cubic fluorite CeO_2 (JCPDS 43-1002) with diffraction peaks at 28.5°, 47.5°, and 56.3° and tetragonal ZrO_2 (JCPDS 50-1089) with *P*42/*nmc* space group diffraction peaks at 30.3°, 50.4°, and 60.2°.[17,18] This indicated that a Ce−Zr solid solution was not formed in the prepared $Ce_1Zr_1O_x$ sample.[11] An explanation for this phenomenon is that stepwise precipitation of $Ce(OH)_3/Ce(OH)_4$ and $Zr(OH)_4$ took place owing to the slow increase in the pH value of the hot Ce−Zr−urea solution during the preparation of the catalysts[19] and subsequently resulted in the formation of CeO_2 and ZrO_2 phases after calcination treatment. For $Ce_1W_{0.5}Zr_1O_x$, no typical XRD diffraction peaks assigned to tungsten oxide or zirconium oxide were detected. The main peaks in the XRD pattern of $Ce_1W_{0.5}Zr_1O_x$ were attributed to *c*-CeO_2, while the intensity of diffraction peaks was decreased compared to $Ce_1Zr_1O_x$. The same phenomenon was also found for the other $Ce_1W_aZr_1O_x$ samples (Figure S3). Rietveld refinement was performed using TOPAS software from BRUKER to obtain precise lattice parameters and crystalline size. It was found that the grain size of $Ce_1W_aZr_1O_x$ was much smaller than that of $Ce_1Zr_1O_x$ (Table S2). Moreover, the lattice parameters of *c*-CeO_2 in $Ce_1W_aZr_1O_x$ obtained by Rietveld refinement were almost equal to those of $Ce_1Zr_1O_x$ (Table S2). The results suggested that ZrO_2 and WO_3 should exist mainly as homogeneously dispersed crystallites or in an amorphous state rather than Ce−Zr or W−Zr solid solutions in $Ce_1W_aZr_1O_x$.[20]

The XRD patterns of hydrothermally aged $Ce_1W_{0.5}Zr_1O_x$-T are shown in Figure 2b. It can be seen that besides the characteristic diffraction peaks of *c*-CeO_2 (PDF 43-1002), solid solution of *t*-$Zr_{0.84}Ce_{0.16}O_2$ (PDF 38-1437) and $Ce_4W_9O_{33}$ (JCPDS 25-0192) appeared for the $Ce_1W_{0.5}Zr_1O_x$-700 catalyst, indicating the occurrence of phase segregation and new phase formation after hydrothermal aging at 700 °C for 16 h. Compared with $Ce_1W_{0.5}Zr_1O_x$-700, little change can be observed for the XRD patterns of $Ce_1W_{0.5}Zr_1O_x$-750, $Ce_1W_{0.5}Zr_1O_x$-800, and $Ce_1W_{0.5}Zr_1O_x$-850. However, it was found by Rietveld refinement that the lattice parameters of cubic CeO_2 decreased and the characteristic peaks corresponding to cubic CeO_2 shifted to a higher value with increasing hydro-

DOI: 10.1021/acs.est.8b03732
Environ. Sci. Technol. 2018, 52, 11769−11777

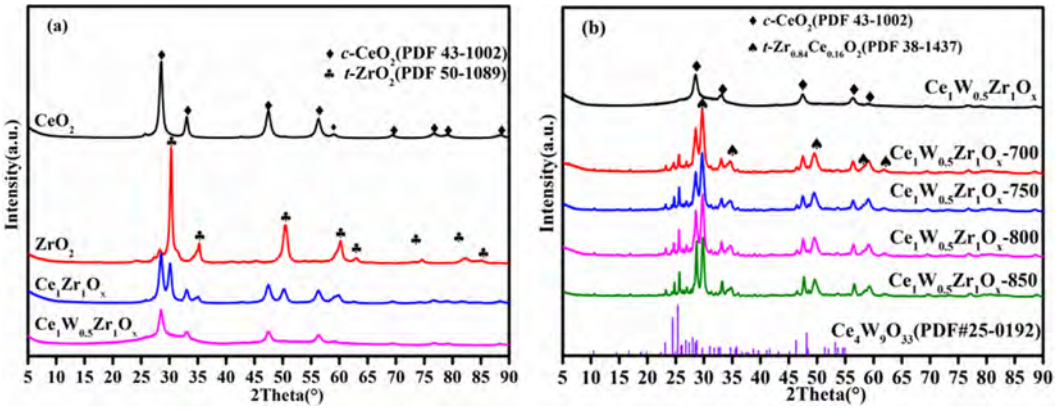

Figure 2. Powder XRD of fresh (a) and hydrothermally aged (b) catalysts.

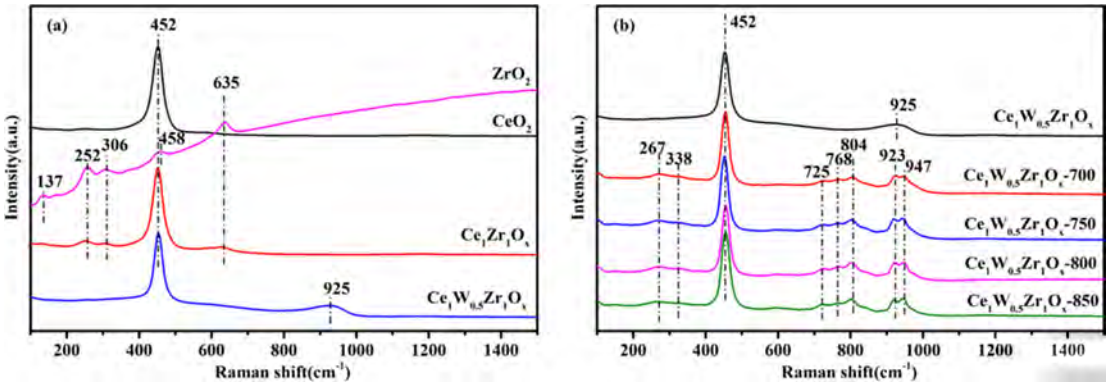

Figure 3. Visible Raman spectrum of fresh (a) and hydrothermally aged (b) catalysts.

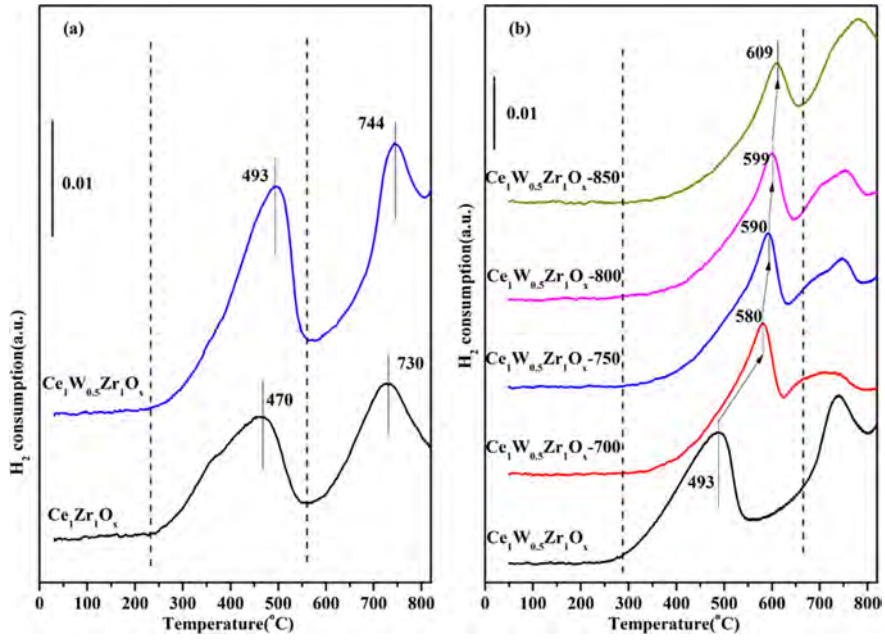

Figure 4. H_2-TPR results of fresh (a) and hydrothermally aged (b) catalysts.

thermal aging temperature (Table S2 and Figure S4). This indicated that a Ce-based ceria−zirconia cubic solid solution formed though the replacement of Ce^{4+} (0.097 nm) by the smaller Zr^{4+} (0.084 nm) owing to the diffusion of ions at a high temperature during the hydrothermal-aging treatment.[20] The formation of a cubic and tetragonal ceria−zirconia solid solution is consistent with the reported ZrO_2−CeO_2 phase diagram below 1400 °C.[21]

Figure 3a shows the Raman spectra of CeO_2, ZrO_2, $Ce_1Zr_1O_x$, and $Ce_1W_{0.5}Zr_1O_x$ samples. One prominent peak at around 452 cm^{-1} can be observed in the Raman spectrum of CeO_2, which can be assigned to the CeO_2 cubic fluorite peak due to the F_{2g}

DOI: 10.1021/acs.est.8b03732
Environ. Sci. Technol. 2018, 52, 11769−11777

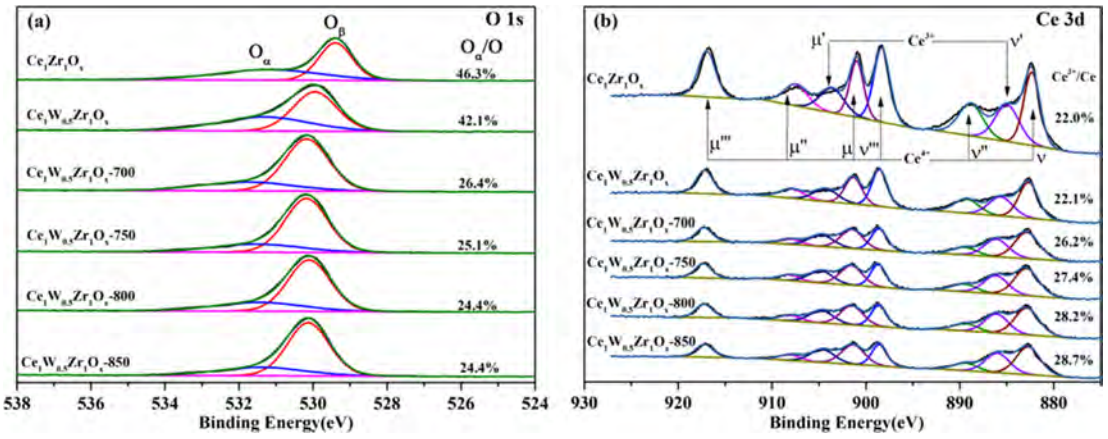

Figure 5. XPS for (a) O 1s and (b) Ce 3d of fresh and hydrothermally aged catalysts.

symmetric breathing mode of oxygen atoms surrounding the cerium ion.[22] The characteristic bands of *t*-ZrO_2 at 137, 252, 306, 458, and 635 cm^{-1} were observed for the ZrO_2 sample.[23] For the $Ce_1Zr_1O_x$ sample, the Raman-active modes of *c*-CeO_2 (452 cm^{-1}) and *t*-ZrO_2 (252, 306, and 635 cm^{-1}) appeared. For the $Ce_1W_{0.5}Zr_1O_x$ catalyst, the intensity of the CeO_2 cubic fluorite peak became weaker, and the bands attributed to *t*-ZrO_2 disappeared. This suggested that the addition of tungsten species inhibited the crystallization of CeO_2 and ZrO_2, in accordance with the results of XRD analysis. In addition, a broad band at around 925 cm^{-1} appeared in the spectrum of $Ce_1W_{0.5}Zr_1O_x$, which could be related to amorphous tungsten oxide or the symmetrical W═O stretching mode of highly dispersed tungsten oxides.[13,24]

The Raman spectra of $Ce_1W_{0.5}Zr_1O_x$-T are shown in Figure 3b. Several new peaks related to tungstate species at 267, 338, 725, 768, 804, 923, and 947 cm^{-1} were observed, which are reported as characteristic bands of $Ce_2(WO_4)_3$.[25,26] However, no $Ce_2(WO_4)_3$ phase was observed in $Ce_1W_{0.5}Zr_1O_x$-T by XRD analysis. It was reported that the mutual transformation of $Ce_4W_9O_{33}$ and $Ce_2(WO_4)_3$ could easily occur at temperatures below 800 °C ($6(Ce_2(WO_4)_3) + O_2 \leftrightharpoons 4CeO_2 + 2(Ce_4W_9O_{33})$).[27] The XRD results of $Ce_1W_{0.5}Zr_1O_x$-T in Figure 2b verified the existence of $Ce_4W_9O_{33}$. Taking these facts into account, we deduced that these Raman modes could be assigned to $Ce_4W_9O_{33}$. This suggests that tungsten species in $Ce_1W_{0.5}Zr_1O_x$-T were mainly in the form of cerium tungstates instead of tungsten trioxide.

3.2. Redox Ability and Surface Species. H_2-TPR was conducted to investigate the reducibility of $Ce_1Zr_1O_x$ and $Ce_1W_{0.5}Zr_1O_x$ catalysts. The amounts of H_2 consumed were determined by the integration of H_2-TPR peaks. As shown in Figure 4a, the $Ce_1Zr_1O_x$ catalyst showed two reduction peaks at around 470 and 730 °C. The H_2 consumption peak at 470 °C was ascribed to the reduction of surface-capping oxygen of Ce^{4+}−O−Ce^{4+} in stoichiometric ceria and the peak centered at ~730 °C was assigned to the reduction of bulk oxygen of Ce^{3+}−O−Ce^{4+} in nonstoichiometric ceria.[6,9] After tungsten addition, the reduction peak of the surface oxygen species on $Ce_1W_{0.5}Zr_1O_x$ shifted to higher temperatures, indicating that the reducibility of $Ce_1W_{0.5}Zr_1O_x$ was attenuated by W doping, in good agreement with previous reports.[20,28] Notably, the amount of H_2 consumption for surface oxygen over $Ce_1W_{0.5}Zr_1O_x$ (373 μmol/g) was higher than that of $Ce_1Zr_1O_x$ (264 μmol/g), suggesting the existence of more reducible surface oxygen species on $Ce_1W_{0.5}Zr_1O_x$ than on $Ce_1Zr_1O_x$. In addition, the reduction peak centered at 744 °C might be attributed to the overlapped reduction peaks of bulk Ce and W.[8]

The H_2-TPR curves of hydrothermally aged $Ce_1W_{0.5}Zr_1O_x$ are shown in Figure 4b. After being hydrothermally aged at 700 °C for 16 h, the reduction peak of surface oxygen showed a shift of ~90 °C to higher reduction temperatures. When further increasing the hydrothermal aging temperature, the reduction peak of surface oxygen shifted slightly to higher temperatures. It is worth noting that severely aged $Ce_1W_{0.5}Zr_1O_x$-850 still retained a certain amount of reducible surface oxygen species. Moreover, the broad peak of $Ce_1W_{0.5}Zr_1O_x$-T above 650 °C, composed of a shoulder peak at lower temperature and a main peak at higher temperature, could be attributed to the overlapping reduction peaks of bulk oxygen species from cerium tungstates and CeO_2. In addition, the hydrogen consumption of bulk oxygen increased in the sequence $Ce_1W_{0.5}Zr_1O_x$-700 < $Ce_1W_{0.5}Zr_1O_x$-750 < $Ce_1W_{0.5}Zr_1O_x$-800 < $Ce_1W_{0.5}Zr_1O_x$-850, which might be due to the formation of Ce−Zr solid solutions, as the inclusion of Zr in the ceria lattice is known to increase the reducibility of the bulk ceria.[29]

XPS measurements were carried out to clarify the chemical state of elements on the surface of fresh and hydrothermally aged catalysts. As shown in Figure 5a, the corresponding O 1s peak could be deconvoluted into two sub-bands: the peak located at around 528.9−530.1 eV was attributed to the lattice oxygen O^{2-} (denoted as O_β), while the one at around 530.8−531.5 eV was assigned to surface oxygen species such as O_2^{2-}(O^-) (denoted as O_α).[18] Surface oxygen O_α is more active in the oxidation of NO to NO_2, which is beneficial to SCR activity via the "fast SCR" reaction.[30] According to the peak-fitting results, the $O_\alpha/(O_\alpha + O_\beta)$ molar ratios of $Ce_1Zr_1O_x$ and $Ce_1W_{0.5}Zr_1O_x$ were 46.3% and 42.1%, respectively. It can be speculated that the $O_\alpha/(O_\alpha + O_\beta)$ ratio was not the decisive factor for the greatly improved NH_3−SCR activity of $Ce_1W_{0.5}Zr_1O_x$. After hydrothermal aging at 700 °C for 16 h, the $O_\alpha/(O_\alpha + O_\beta)$ molar ratio of $Ce_1W_{0.5}Zr_1O_x$-700 was 26.4%, which was decreased almost by 50% compared to that of $Ce_1W_{0.5}Zr_1O_x$. However, with the further increase of the hydrothermal aging temperature, little change of the $O_\alpha/(O_\alpha + O_\beta)$ molar ratio could be found. Even after being hydrothermally aged at 850 °C for 16 h, $Ce_1W_{0.5}Zr_1O_x$-850 still contained a certain amount of surface oxygen O_α.

Figure 5b exhibits the Ce 3d XPS results. The peaks labeled μ, μ″, μ‴, ν, ν″, and ν‴ represent Ce^{4+}, and the peaks labeled μ′ and

DOI: 10.1021/acs.est.8b03732
Environ. Sci. Technol. 2018, 52, 11769−11777

ν' are associated with Ce^{3+}.[9] It could be concluded that Ce^{4+} and Ce^{3+} coexisted on the surface of all catalysts. The Ce^{3+}/Ce ratios were calculated by the following formula:[31]

$$Ce^{3+}/(Ce^{3+} + Ce^{4+})\ (\%) = \frac{S(\mu') + S(\nu')}{\sum [S(\mu) + S(\nu)]} \times 100$$

It was reported that the main source of Ce^{3+} in CeO_2-based catalysts is the intrinsic O_v of reduced CeO_2, which has a positive correlation with surface oxygen species, thus Ce^{3+}/Ce and O_α/O should have identical rising/falling trends.[32] In this study, $Ce_1W_{0.5}Zr_1O_x$ and $Ce_1Zr_1O_x$ possessed equal Ce^{3+}/Ce ratios, while the O_α/O of $Ce_1W_{0.5}Zr_1O_x$ was lower than that of $Ce_1Zr_1O_x$. In addition, the Ce^{3+}/Ce ratio increased and the O_α/O ratio decreased with increasing hydrothermal aging temperature. We deduce that the microcrystalline or amorphous $Ce^{3+}-O-W^{6+}$ oxides in $Ce_1W_{0.5}Zr_1O_x$ and crystalline $Ce_4W_9O_{33}$ in $Ce_1W_{0.5}Zr_1O_x$-T (verified by XRD and Raman) represent another source of Ce^{3+}.[33] The Zr 3d and W 4f spectra of $Ce_1W_{0.5}Zr_1O_x$ and $Ce_1W_{0.5}Zr_1O_x$-T showed little difference, suggesting that hydrothermal aging treatment did not influence the valence states of tungsten and zirconium. (Figure S5)

3.3. Surface Acidity. NH_3-TPD was carried out to investigate the acidic properties of the catalysts. As shown in Figure 6, three overlapping peaks can be observed in the NH_3 desorption profile of $Ce_1Zr_1O_x$. The NH_3 desorption peaks centered at 138 °C should originate from ionic NH_4^+ coordinated to weak Brønsted acid sites.[16,34] Since it is very difficult to identify the strong Brønsted acid sites and Lewis acid sites according to the NH_3-TPD profiles, both the peaks centered at 202 and 252 °C were ascribed to strong acid sites.[34] Compared with $Ce_1Zr_1O_x$, the NH_3 desorption profiles of $Ce_1W_{0.5}Zr_1O_x$ and $Ce_1W_{0.5}Zr_1O_x$-T moved to higher temperature by about 20 °C, indicating their stronger acid strength than that of $Ce_1Zr_1O_x$ catalysts. In addition, the NH_3 desorption amounts were 8.54×10^{-5} mol/g for $Ce_1Zr_1O_x$ and 2.10×10^{-4} mol/g for $Ce_1W_{0.5}Zr_1O_x$, respectively. This meant that the NH_3 storage capacity of the cerium/zirconium mixed oxides was greatly increased by the addition of W. After hydrothermal aging treatment at 700 °C for 16 h, the NH_3 desorption amount of $Ce_1W_{0.5}Zr_1O_x$-700 was 6.59×10^{-5} mol/g. Further increasing the hydrothermal aging temperature to 850 °C, the NH_3 desorption amount of $Ce_1W_{0.5}Zr_1O_x$-850 was 6.08×10^{-5} mol/g, which was close to that of $Ce_1W_{0.5}Zr_1O_x$-700. When normalized to the surface area, the NH_3 desorption amounts per unit area for $Ce_1W_{0.5}Zr_1O_x$-700 and $Ce_1W_{0.5}Zr_1O_x$-850 are 3.97×10^{-6} mol/(m^2) and 5.96×10^{-6} mol/(m^2), respectively, which are higher than that of 1.17×10^{-6} mol/(m^2) for $Ce_1Zr_1O_x$ and 2.28×10^{-6} mol/(m^2) for $Ce_1W_{0.5}Zr_1O_x$. This meant that W addition and hydrothermal-aging treatment even have promoting effects on the acid site density.

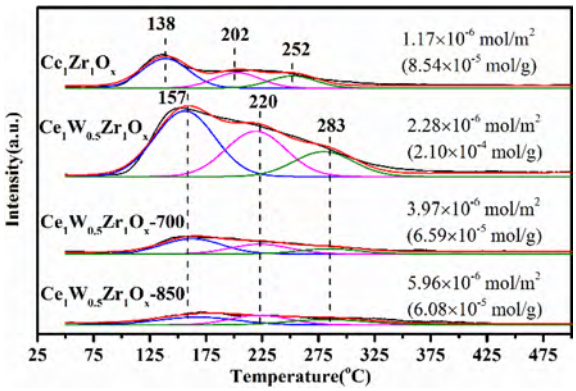

Figure 6. NH_3-TPD patterns for the $Ce_1Zr_1O_x$, $Ce_1W_{0.5}Zr_1O_x$, $Ce_1W_{0.5}Zr_1O_x$-700, and $Ce_1W_{0.5}Zr_1O_x$-850 catalysts.

In order to further investigate the surface acid sites, the *in situ* DRIFTS of NH_3 adsorption was carried out. Figure 7a shows the spectra of NH_3 species chemically adsorbed onto $Ce_1Zr_1O_x$ and $Ce_1W_{0.5}Zr_1O_x$ at 200 °C. The bands at 1602 and 1224 cm^{-1} and 1186 cm^{-1} were attributed to the asymmetric and symmetric bending vibrations of N−H bonds in the NH_3 coordinated to Lewis acid sites, respecitvely, while the bands at 1681 and 1433 cm^{-1} and 1440 and 1415 cm^{-1} can be ascribed to the symmetric and asymmetric bending vibrations of N−H bonds in NH_4^+ chemisorbed on Brønsted acid sites, respectively.[34,35] The negative bands at 3658 and 3766 cm^{-1} can be ascribed to the O−H stretching mode in the surface hydroxyl groups, which could also represent Brønsted acid sites.[36] The three small peaks in the range of 3168−3350 cm^{-1} corresponded to the N−H stretching vibration modes of NH_3 coordinated to the Lewis acid sites.[17] The addition of tungsten to $Ce_1Zr_1O_x$ markedly increased the amount of both Brønsted and Lewis acid sites. According to Li et al.'s report,[37] the Lewis acid sites should originate from CeO_2 and some of the unsaturated W^{n+} cations of WO_3 crystallites; additionally, the Brønsted acid sites formed on the W−O−W or W═O sites of $Ce_4W_9O_{33}$. In addition, the main difference

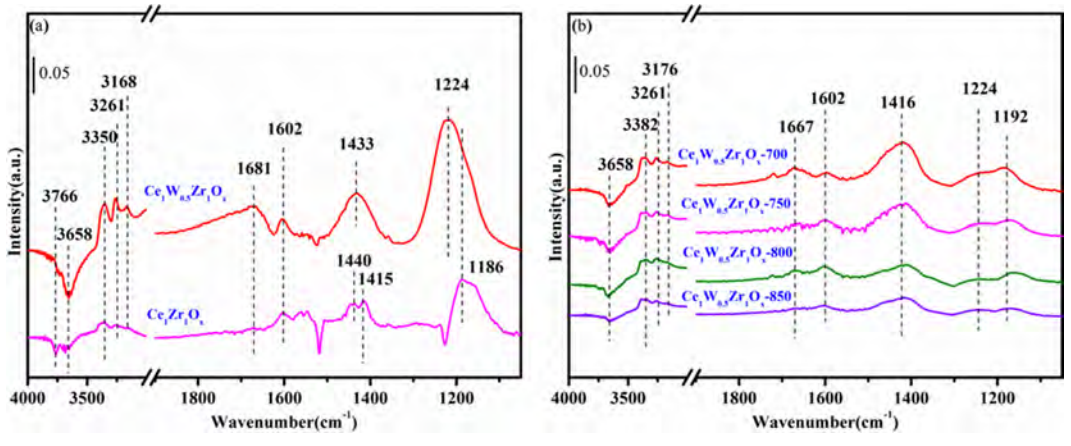

Figure 7. *In situ* DRIFTS of NH_3 adsorption of fresh (a) and hydrothermally aged (b) catalysts at 200 °C.

DOI: 10.1021/acs.est.8b03732
Environ. Sci. Technol. 2018, 52, 11769−11777

between the spectra of $Ce_1Zr_1O_x$ and $Ce_1W_{0.5}Zr_1O_x$ lies in the band attributed to Lewis acid sites: a blue shift occurred from $Ce_1Zr_1O_x$ (1186 cm^{-1}) to $Ce_1W_{0.5}Zr_1O_x$ (1224 cm^{-1}), verifying that extra Lewis acid sites for NH_3 adsorption were induced by WO_x species.[38] The acidic properties of hydrothermally aged $Ce_1W_{0.5}Zr_1O_x$ catalysts were also investigated by *in situ* NH_3 adsorption DRIFTS. As shown in Figure 7b, the intensity of the bands attributed to Brønsted acid sites (1416, 1667 cm^{-1}) and Lewis acid sites (1192, 1602, and 1224 cm^{-1}) decreased after hydrothermal aging.

3.4. Interaction of the W and Ce in $Ce_1W_{0.5}Zr_1O_x$. Acidity and redox ability are both important for catalysts in the SCR reaction. The significant enhancement of SCR activity for Ce−Zr materials by doping with WO_3 was mainly attributed to the promotion of acidity in previous reports.[20] In this work, the W addition to $Ce_1Zr_1O_x$ significantly increased the Brønsted acid sites and Lewis acid sites, according to the results of NH_3-TPD and *in situ* DRIFTS of NH_3 adsorption. In addition, ceria is considered to be an active species in ceria−zirconia-based SCR catalysts due to its redox cycle between Ce^{3+} and Ce^{4+}.[17] In the current study, the addition of W to $Ce_1Zr_1O_x$ decreased the Ce surface atomic concentration with almost no change in the Ce^{3+}/Ce molar ratio (Table S3 and Figure 5a), indicating that $Ce_1W_{0.5}Zr_1O_x$ should contain fewer redox sites on the surface than $Ce_1Zr_1O_x$. The H_2-TPR results suggested that $Ce_1W_{0.5}Zr_1O_x$ had a higher reduction temperature than $Ce_1Zr_1O_x$, which suggested lowered reducibility after tungsten addition (Figure 4a). Moreover, fewer surface nitrate species were formed on $Ce_1W_{0.5}Zr_1O_x$ compared with $Ce_1Zr_1O_x$, according to the results of *in situ* DRIFTS of NO + O_2 adsorption (Figure S6). The NO conversion of $Ce_1W_{0.5}Zr_1O_x$ during NO oxidation experiments was much lower than that of $Ce_1Zr_1O_x$ over the whole temperature range (Figure S7). Therefore, W addition to $Ce_1Zr_1O_x$ had no promotional effects on the redox ability.

According to the XPS and XRF results (Table S3), the surface atomic ratio of Ce/Zr in $Ce_1Zr_1O_x$ (4.1) was much higher than its bulk atomic ratio (0.9). This indicated that CeO_2 tended to be distributed on the surface, while ZrO_2 served as the bulk phase in $Ce_1Zr_1O_x$. For $Ce_1W_{0.5}Zr_1O_x$, the surface atomic ratio of Ce/Zr decreased to 0.8, which was approximately equal to its bulk Ce/Zr atomic ratio (0.9). In addition, the surface atomic ratio of W/Ce (0.5) was equal to its bulk W/Ce atomic ratio (0.5). The results indicated that the addition of tungsten stabilized W species and promoted the formation of a homogeneous Ce−W−Zr system with no phase separation on the surface.[39] Recently, Iwasaki et al. proposed that the existence of large amounts of interfacial acidic-redox sites from the interaction of Ce with WO_3 was critical to the higher SCR activity of WO_3/CeO_2 than a mixture of CeO_2 and WO_3/ZrO_2.[13] In our work, the WO_3 content in $Ce_1W_{0.5}Zr_1O_x$ was around 26 wt % according to XRF characterization. We prepared 26 wt % $WO_3/Ce_1Zr_1O_x$ by the wet impregnation method for comparison. It was found that the NOx conversion of $Ce_1W_{0.5}Zr_1O_x$ was much higher than that of 26 wt % $WO_3/Ce_1Zr_1O_x$ (Figure S8). Taking these things into account, we deduce that the interaction of the W and Ce in $Ce_1W_{0.5}Zr_1O_x$ resulted in the tight coupling and homogeneous dispersion of redox-acid sites, which are critical for the SCR reaction.[13,20]

3.5. Hydrothermal Stability. After hydrothermal aging, a significant decrease in surface area and acidity as well as new phase formation occurred for $Ce_1W_{0.5}Zr_1O_x$, and those factors might make the main contribution to the decrease in the low temperature activity of this catalyst. The SCR reaction rates were normalized by the surface specific area in consideration of the big difference in BET area between $Ce_1W_{0.5}Zr_1O_x$ and $Ce_1W_{0.5}Zr_1Ox$-T, and the real SCR reaction rates are also shown in Table 1. The data showed that the reaction rates per unit area of $Ce_1W_{0.5}Zr_1O_x$-T were higher than that of $Ce_1W_{0.5}Zr_1O_x$. It is worth noting that little difference in SCR reaction rates was observed for $Ce_1W_{0.5}Zr_1O_x$-T hydrothermally aged in the temperature range of 700−850 °C.

The apparent activation energy of a catalytic reaction is a significant factor in evaluating the role of a catalyst in the catalytic reaction and the efficiency of the catalyst.[40] Steady-state kinetics studies were carried out for $Ce_1W_{0.5}Zr_1O_x$, $Ce_1W_{0.5}Zr_1O_x$-700, and $Ce_1W_{0.5}Zr_1O_x$-850, and the Arrhenius plots of ln *R* against 1000 times the inverse temperature (1000/T) are presented in Figure 8. An apparent activation energy of

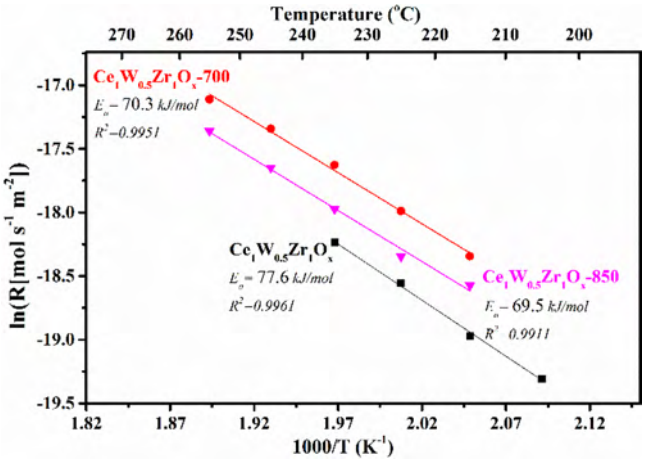

Figure 8. Kinetic results of NH_3−SCR over the fresh and hydrothermally aged $Ce_1W_{0.5}Zr_1O_x$ catalysts.

70.3 kJ/mol was obtained for the NH_3−SCR reaction over the $Ce_1W_{0.5}Zr_1O_x$-700 catalyst, which was slightly lower than that of $Ce_1W_{0.5}Zr_1O_x$ (77.6 kJ/mol). Further increasing the hydrothermal aging temperature had no influence on the apparent activation energy of $Ce_1W_{0.5}Zr_1O_x$-850 (69.5 kJ/mol). Therefore, the reaction path should be unaffected by the hydrothermal aging treatment in consideration of the similar apparent activation energy barriers.

Taking these things into account, the excellent SCR activity of $Ce_1W_{0.5}Zr_1Ox$-T should be attributed to the Ce−W active sites and the stability of its structure. On one hand, the formation of Ce−W oxide species, mainly $Ce_4W_9O_{33}$, could provide tighter coupling of acid-redox sites, which have been proven to possess higher intrinsic activity.[22] However, the exposure of Ce−W oxide species, which can be involved in the SCR reaction, was limited due to the low surface area of hydrothermally aged $Ce_1W_{0.5}Zr_1O_x$ catalysts. On the other hand, the XRD, Raman, and N_2 physical adsorption results showed that changes in the textural properties of $Ce_1W_{0.5}Zr_1O_x$-T after hydrothermal aging at 700−850 °C were insignificant. The TG-DSC results of $Ce_1W_{0.5}Zr_1O_x$ showed that a sharp exothermic peak at 683 °C could be observed in the DSC curve (Figure S9). This suggested that the transition of ZrO_2 from the amorphous phase to thermostable tetragonal $Zr_{0.84}Ce_{0.16}O_2$ occurred.[41,42] Although the crystallite grain size of $Ce_1W_{0.5}Zr_1O_x$ tended to increase after the hydrothermal aging treatment, it was much smaller than that of the hydrothermally aged $Ce_1Zr_1O_x$ catalyst under the same

DOI: 10.1021/acs.est.8b03732
Environ. Sci. Technol. 2018, 52, 11769−11777

hydrothermal aging temperature (Table S2). The thermal stability of tetragonal $Zr_{0.84}Ce_{0.16}O_2$ might also contribute to the hydrothermal stability of $Ce_1W_{0.5}Zr_1Ox$-T.[11]

■ ASSOCIATED CONTENT

Supporting Information

The Supporting Information is available free of charge on the ACS Publications website at DOI: 10.1021/acs.est.8b03732.

Information regarding catalyst preparation details, characterization methods, N_2 selectivity during SCR reaction, *in situ* DRIFTS of NO + O_2 adsorption, NO oxidation, TG-DSC, and additional results (PDF)

■ AUTHOR INFORMATION

Corresponding Author

*Tel.: +86 10 62849123. E-mail: honghe@rcees.ac.cn.

ORCID

Jingjing Liu: 0000-0002-8719-6354
Yulong Shan: 0000-0002-5031-8522
Yunbo Yu: 0000-0003-2935-0955

Notes

The authors declare no competing financial interest.

■ ACKNOWLEDGMENTS

This work was financially supported by the Key Project of National Natural Science Foundation (21637005), the National Natural Science Foundation of China (21777174, 51822811), and the National Key R&D Program of China (2017YFC0211105).

■ REFERENCES

(1) Rohart, E.; Krocher, O.; Casapu, M.; Marques, R.; Harris, D.; Jones, C. Acidic Zirconia Mixed Oxides for NH_3-SCR Catalysts for PC and HD Applications. *SAE Tech. Pap. Ser.* **2011**, *1*, DOI: 10.4271/2011-01-1327.

(2) Schmieg, S. J.; Oh, S. H.; Kim, C. H.; Brown, D. B.; Lee, J. H.; Peden, C. H.; Kim, D. H. Thermal durability of Cu-CHA NH_3-SCR catalysts for diesel NOx reduction. *Catal. Today* **2012**, *184*, 252−261.

(3) Liu, F. D.; Yu, Y. B.; He, H. Environmentally-benign catalysts for the selective catalytic reduction of NOx from diesel engines: structure-activity relationship and reaction mechanism aspects. *Chem. Commun.* **2014**, *50*, 8445−8463.

(4) Liu, F. D.; Asakura, K.; He, H.; Liu, Y. C.; Shan, W. P.; Shi, X. Y.; Zhang, C. B. Influence of calcination temperature on iron titanate catalyst for the selective catalytic reduction of NOx with NH_3. *Catal. Today* **2011**, *164*, 520−527.

(5) Colon, G.; Valdivieso, F.; Pijolat, M.; Baker, R. T.; Calvino, J. J.; Bernal, S. Textural and phase stability of $Ce_xZr_{1-x}O_2$ mixed oxides under high temperature oxidizing conditions. *Catal. Today* **1999**, *50*, 271−284.

(6) Si, Z. C.; Weng, D.; Wu, X. D.; Ran, R.; Ma, Z. R. NH_3-SCR activity, hydrothermal stability, sulfur resistance and regeneration of $Ce_{0.75}Zr_{0.25}O_2$-PO_4^{3-} catalyst. *Catal. Commun.* **2012**, *17*, 146−149.

(7) Baidya, T.; Bernhard, A.; Elsener, M.; Kröcher, O. Hydrothermally Stable WO_3/ZrO_2-$Ce_{0.6}Zr_{0.4}O_2$ Catalyst for the Selective Catalytic Reduction of NO with NH_3. *Top. Catal.* **2013**, *56*, 23−28.

(8) Li, J. Y.; Song, Z. X.; Ning, P.; Zhang, Q. L.; Liu, X.; Li, H.; Huang, Z. Z. Influence of calcination temperature on selective catalytic reduction of NOx with NH_3 over CeO_2-ZrO_2-WO_3 catalyst. *J. Rare Earths* **2015**, *33*, 726−735.

(9) Ning, P.; Song, Z. X.; Li, H.; Zhang, Q. L.; Liu, X.; Zhang, J. H.; Tang, X. S.; Huang, Z. Z. Selective catalytic reduction of NO with NH_3 over CeO_2-ZrO_2-WO_3 catalysts prepared by different methods. *Appl. Surf. Sci.* **2015**, *332*, 130−137.

(10) Song, Z. X.; Ning, P.; Zhang, Q. L.; Li, H.; Zhang, J. H.; Wang, Y. C.; Liu, X.; Huang, Z. Z. Activity and hydrothermal stability of CeO_2-ZrO_2-WO_3 for the selective catalytic reduction of NOx with NH_3. *J. Environ. Sci.* **2016**, *42*, 168−177.

(11) Ding, S. P.; Liu, F. D.; Shi, X. Y.; He, H. Promotional effect of Nb additive on the activity and hydrothermal stability for the selective catalytic reduction of NOx with NH_3 over $CeZrO_x$ catalyst. *Appl. Catal., B* **2016**, *180*, 766−774.

(12) Li, Y.; Cheng, H.; Li, D. Y.; Qin, Y. S.; Xie, Y. M.; Wang, S. D. WO_3/CeO_2-ZrO_2, a promising catalyst for selective catalytic reduction (SCR) of NOx with NH_3 in diesel exhaust. *Chem. Commun.* **2008**, 1470−1472.

(13) Iwasaki, M.; Dohmae, K.; Nagai, Y.; Sudo, E.; Tanaka, T. Experimental assessment of the bifunctional NH_3-SCR pathway and the structural and acid-base properties of WO_3 dispersed on CeO_2 catalysts. *J. Catal.* **2018**, *359*, 55−67.

(14) Xu, G. Y.; Ma, J. Z.; He, G. Z.; Yu, Y. B.; He, H. An alumina-supported silver catalyst with high water tolerance for H_2 assisted C_3H_6-SCR of NOx. *Appl. Catal., B* **2017**, *207*, 60−71.

(15) Usberti, N.; Jablonska, M.; Blasi, M. D.; Forzatti, P.; Lietti, L.; Beretta, A. Design of a "high-efficiency" NH_3-SCR reactor for stationary applications. A kinetic study of NH_3 oxidation and NH_3-SCR over V-based catalysts. *Appl. Catal., B* **2015**, *179*, 185−195.

(16) Zhan, S. H.; Zhang, H.; Zhang, Y.; Shi, Q.; Li, Y.; Li, X. J. Efficient NH_3-SCR removal of NOx with highly ordered mesoporous WO_3-CeO_2 at low temperatures. *Appl. Catal., B* **2017**, *203*, 199−209.

(17) Gao, S.; Wang, P. L.; Yu, F. X.; Wang, H. Q.; Wu, Z. B. Dual resistance to alkali metals and SO_2: vanadium and cerium supported on sulfated zirconia as an efficient catalyst for NH_3-SCR. *Catal. Sci. Technol.* **2016**, *6*, 8148−8156.

(18) Zhao, L. K.; Li, C. T.; Li, S. H.; Wang, Y.; Zhang, J. Y.; Wang, T.; Zeng, G. M. Simultaneous removal of elemental mercury and NO in simulated flue gas over V_2O_5/ZrO_2-CeO_2 catalyst. *Appl. Catal., B* **2016**, *198*, 420−430.

(19) Huang, H. L.; Shan, W. P.; Yang, S. J.; Zhang, J. H. Novel approach for a cerium-based highly efficient catalyst with excellent NH_3-SCR performance. *Catal. Sci. Technol.* **2014**, *4*, 3611−3614.

(20) Can, F.; Berland, S.; Royer, S.; Courtois, X.; Duprez, D. Composition-Dependent Performance of $Ce_xZr_{1-x}O_2$ Mixed-Oxide-Supported WO_3 Catalysts for the NOx Storage Reduction-Selective Catalytic Reduction Coupled Process. *ACS Catal.* **2013**, *3*, 1120−1132.

(21) Tani, E.; Yoshimura, M.; Somiya, S. Revised phase diagram of the system ZrO_2-CeO_2 below 1400 °C. *J. Am. Ceram. Soc.* **1983**, *66*, 506−510.

(22) Peng, Y.; Si, W. Z.; Li, X.; Chen, J. J.; Li, J. H.; Crittenden, J.; Hao, J. M. Investigation of the Poisoning Mechanism of Lead on the CeO_2-WO_3 Catalyst for the NH_3-SCR Reaction via in Situ IR and Raman Spectroscopy Measurement. *Environ. Sci. Technol.* **2016**, *50*, 9576−9582.

(23) Li, M. J.; Feng, Z. C.; Xiong, G.; Ying, P. L.; Xin, Q.; Li, C. Phase transformation in the surface region of zirconia detected by UV Raman spectroscopy. *J. Phys. Chem. B* **2001**, *105*, 8107−8111.

(24) Santato, C.; Odziemkowski, M.; Ulmann, M.; Augustynski, J. Crystallographically oriented mesoporous WO_3 films: synthesis, characterization, and applications. *J. Am. Chem. Soc.* **2001**, *123*, 10639−10649.

(25) Burcham, L. J.; Wachs, I. E. Vibrational analysis of the two non-equivalent, tetrahedral tungstate (WO_4) units in $Ce_2(WO_4)_3$ and $La_2(WO_4)_3$. *Spectrochim. Acta, Part A* **1998**, *54*, 1355−1368.

(26) Mamede, A. S.; Payen, E.; Grange, P.; Poncelet, G.; Ion, A.; Alifanti, M.; Pârvulescu, V. I. Characterization of WO_x/CeO_2 catalysts and their reactivity in the isomerization of hexane. *J. Catal.* **2004**, *223*, 1−12.

(27) Yoshimura, M.; Sibieude, F.; Rouanet, A.; Foex, M. Identification of binary compounds in the system Ce_2O_3-WO_3. *J. Solid State Chem.* **1976**, *16*, 219−232.

(28) Ma, Z. R.; Weng, D.; Wu, X. D.; Si, Z. C. Effects of WO_x modification on the activity, adsorption and redox properties of CeO_2

DOI: 10.1021/acs.est.8b03732
Environ. Sci. Technol. 2018, 52, 11769−11777

catalyst for NOx reduction with ammonia. *J. Environ. Sci.* **2012**, *24*, 1305−1316.
(29) Cheng, Y.; Song, W. Y.; Liu, J.; Zheng, H. L.; Zhao, Z.; Xu, C. M.; Wei, Y. C.; Hensen, E. J. M. Simultaneous NOx and Particulate Matter Removal from Diesel Exhaust by Hierarchical Fe-Doped Ce-Zr Oxide. *ACS Catal.* **2017**, *7*, 3883−3892.
(30) Shan, W. P.; Liu, F. D.; He, H.; Shi, X. Y.; Zhang, C. B. A superior Ce-W-Ti mixed oxide catalyst for the selective catalytic reduction of NOx with NH_3. *Appl. Catal., B* **2012**, *115*, 100−106.
(31) Xu, H. D.; Feng, X.; Liu, S.; Wang, Y.; Sun, M. M.; Wang, J. L.; Chen, Y. Q. Promotional effects of Titanium additive on the surface properties, active sites and catalytic activity of $W/CeZrO_x$ monolithic catalyst for the selective catalytic reduction of NOx with NH_3. *Appl. Surf. Sci.* **2017**, *419*, 697−707.
(32) Shan, W. P.; Liu, F. D.; He, H.; Shi, X. Y.; Zhang, C. B. Novel Cerium-Tungsten mixed oxide catalyst for the selective catalytic reduction of NOx with NH_3. *Chem. Commun.* **2011**, *47*, 8046−8048.
(33) Peng, Y.; Li, K. Z.; Li, J. H. Identification of the active sites on CeO_2-WO_3 catalysts for SCR of NOx with NH_3: An in situ IR and Raman spectroscopy study. *Appl. Catal., B* **2013**, *140*−*141*, 483−492.
(34) Zhao, X.; Huang, L.; Li, H. R.; Hu, H.; Hu, X. N.; Shi, L. Y.; Zhang, D. S. Promotional effects of zirconium doped $CeVO_4$ for the low-temperature selective catalytic reduction of NOx with NH_3. *Appl. Catal., B* **2016**, *183*, 269−281.
(35) Chen, L.; Li, J. H.; Ge, M. F. DRIFT study on Cerium-Tungsten/Titiania catalyst for selective catalytic reduction of NOx with NH_3. *Environ. Sci. Technol.* **2010**, *44*, 9590−9596.
(36) Ma, Z. R.; Wu, X. D.; Härelind, H.; Weng, D.; Wang, B. D.; Si, Z. C. NH_3-SCR reaction mechanisms of $NbO_x/Ce_{0.75}Zr_{0.25}O_2$ catalyst: DRIFTS and kinetics studies. *J. Mol. Catal. A: Chem.* **2016**, *423*, 172−180.
(37) Li, X.; Li, J. H.; Peng, Y.; Li, X. S.; Li, K. Z.; Hao, J. M. Comparison of the Structures and Mechanism of Arsenic Deactivation of CeO_2-MoO_3 and CeO_2-WO_3 SCR Catalysts. *J. Phys. Chem. C* **2016**, *120*, 18005−18014.
(38) Michalow-Mauke, K. A.; Lu, Y.; Kowalski, K.; Graule, T.; Nachtegaal, M.; Kröcher, O.; Ferri, D. Flame-Made WO_3/CeO_x-TiO_2 Catalysts for Selective Catalytic Reduction of NOx by NH_3. *ACS Catal.* **2015**, *5*, 5657−5672.
(39) Bozo, C.; Gaillard, F.; Guilhaume, N. Characterisation of Ceria-Zirconia solid solutions after hydrothermal ageing. *Appl. Catal., A* **2001**, *220*, 69−77.
(40) Xu, H. D.; Li, Y. S.; Xu, B. Q.; Cao, Y.; Feng, X.; Sun, M. M.; Gong, M. C.; Chen, Y. Q. Effectively promote catalytic performance by adjusting W/Fe molar ratio of $FeW_x/Ce_{0.68}Zr_{0.32}O_2$ monolithic catalyst for NH_3-SCR. *J. Ind. Eng. Chem.* **2016**, *36*, 334−345.
(41) Sohn, J. R.; Kim, J. G.; Kwon, T. D.; Park, E. H. Characterization of Titanium Sulfate Supported on Zirconia and Activity for Acid Catalysis. *Langmuir* **2002**, *18*, 1666−1673.
(42) Wang, Q. Y.; Zhao, B.; Li, G. F.; Zhou, R. X. Application of rare earth modified Zr-based Ceria-Zirconia solid solution in three-way catalyst for automotive emission control. *Environ. Sci. Technol.* **2010**, *44*, 3870−3875.

DOI: 10.1021/acs.est.8b03732
Environ. Sci. Technol. 2018, 52, 11769−11777